Materials Physics and Mechanics. 2022;50(2): 226-238
Research article
http://dx.doi.org/10.18149/MPM.5022022_4

Submitted: May 7, 2022
Approved: September 1 2022
Accepted: October 5, 2022

Wave propagation under the influence of voids and non-free surfaces in a micropolar elastic medium

Sachin Kaushal[1]✉, Rajneesh Kumar[2], Arun Kochar[1]

[1]Department of Mathematics, School of Chemical Engineering and Physical Sciences, Lovely Professional University, Phagwara, India

[2]Department of Mathematics, Kurukshetra University, Kurukshetra, India

✉ sachin_kuk@yahoo.co.in

Abstract. A problem of reflection of elastic wave in micropolar media with the void at non-free surface is considered. The governing equations are formulated for a specific model. The equations so obtained are put in two dimensions and converted into dimensionless form and then solved with the help of the reflection technique. Non-free boundary conditions are taken to obtain the amplitude ratios of different reflected waves i.e. Longitudinal displacement wave (LD-wave), Longitudinal void volume fraction wave (LVVF-wave), Transverse wave (T-wave), and Micro-rotational wave (MR-wave). These amplitude ratios are obtained numerically and also shown graphically for the non-free surface as well as for the free surface to depict the impact of stiffness and void. From the present study, certain cases are also deduced.

Keywords: wave propagation, non-free surface, micropolar, void, amplitude ratio

***Acknowledgements**. No external funding was received for this study.*

Citation: Kaushal S, Kumar R, Kochar A. Wave propagation under the influence of voids and non-free surfaces in a micropolar elastic medium. *Materials Physics and Mechanics*. 2022;50(2): 226-238. DOI: 10.18149/MPM.5022022_4.

1. Introduction

When a plane wave traveling through an elastic medium comes across a boundary surface of the medium, it gets reflected into the medium. This phenomenon occurs in many situations, e.g. seismology, engineering, optics, etc. The investigation of the reflection problem of plane waves is an important tool to analyze various properties of the medium. For example, such problems find applications in the field of seismology as a method for determining the characteristics of the earth's internal structure as well as for the exploration of valuable materials. Various authors have contributed to the field of elasticity and wave propagation, notable of them are [1-8].

An elastic material that consists of small pores is defined as linear elastic material with voids. In the classical theory of elasticity, the volume of such pores is neglected which plays an important role as the volume of such pores is to be taken as an independent kinematic variable. Nunziato and Cowin [9] developed a theory that is based on non-linear elastic material having voids. Later on, Cowin and Nunziato [10] extended this to a linear elastic material having pores. Various authors have done different research on micropolar elastic material with void and notable them are [11-16].

In the context of micropolar porous media Marin [17] formulated a heat-flux theory that includes the heat-flux vector and an evolution equation for it. Lianngenga [18] studied the problem of attenuations and phase velocities of plane body waves and their reflection from a stress-free surface in the micropolar material with voids and also computed amplitude as well as energy ratios of reflected waves. Kumari and Kaliraman [19] observed variation in modulus of amplitude ratios of various reflected and refracted waves against incident waves traveling at high frequency as well as at low frequency in micropolar elastic solid with a void. Marin et al. [20] showed that the solution of mixed IBVP (initial boundary value problem) for porous micropolar bodies depends continuously on coefficients that couple the micropolar deformation equations. With the help of normal mode analysis, Alharbi et al. [21] obtained the expression for the components of stress, displacement components, microrotation components, and temperature field and also studied the effect of heat source on these expressions in the micropolar medium with void under the theory of the three-phase-lag model of thermoelasticity.

In the above-mentioned work, it is observed that the reflection of waves in micropolar elastic wave medium is usually taken over the free surface. However, In actual engineering problems due to accumulative damage, the interface may be imperfect and it will lead to a non-free surface with distributed elastic constraint or support. The study of the non-free surface is at the incubating stage. Zhang et al. [22] calculated energy flux ratios of reflected waves at the non-free surface of a micropolar elastic half-space. Singh [23] calculated reflection coefficients of thermoelastic waves by assuming different boundary conditions at the non-free surface.

The concept of a non-free surface is also used in various fields of Physics such as acoustics and electromagnetism therefore a problem on the boundary surface is considered as non-free with a micropolar elastic constraint with the void, where each mass point is subjected to the normal, tangential and rotational stiffnesses. The amplitude ratios of reflected waves are calculated for the desired boundary conditions at a non-free surface. The impact of voids and the influence of the non-free surface on amplitude ratios are shown graphically against the angle of incidence.

2. Governing equations

The field equations and constitutive relations in absence of body forces, body couples, and heat source (Eringen [24] and Iesan [25]) are as follows:

$$(\lambda+\mu)\nabla(\nabla.\vec{u})+(\mu+K)\nabla^2\vec{u}+K(\nabla\times\vec{\phi})+\beta^*\nabla q=\rho\frac{\partial^2\vec{u}}{\partial t^2}, \tag{1}$$

$$(\alpha+\beta)\nabla(\nabla.\vec{\phi})+\gamma\nabla^2\vec{\phi}+K(\nabla\times\vec{u})-2K\vec{\phi}=\rho\hat{j}\frac{\partial^2\vec{\phi}}{\partial t^2}, \tag{2}$$

$$\alpha^*\nabla^2 q-\omega^*\dot{q}-\xi^* q-\beta^*(\nabla.\vec{u})=\rho\kappa^*\frac{\partial^2 q}{\partial t^2}, \tag{3}$$

$$t_{ij}=\lambda u_{r,r}\delta_{ij}+\mu(u_{i,j}+u_{j,i})+K(u_{j,i}-\varepsilon_{ijr}\phi_r)+\beta^* q\delta_{ij}, \tag{4}$$

$$m_{ij}=\alpha\phi_{r,r}\delta_{ij}+\beta\phi_{i,j}+\gamma\phi_{j,i}, \tag{5}$$

where λ,μ are Lame's constants, t is time, t_{ij} are stress components, q denotes volume fraction field, δ_{ij} is Kronecker delta, ρ is density, $\vec{u}$ is displacement vector, $\vec{\phi}$ denotes microrotation vector, ε_{ijr} is an alternating tensor, α,β,γ,K are micropolar constants, $\hat{j}$ denotes micro-inertia, m_{ij} denotes component of couple stress tensor, $\omega^*,\beta^*,\alpha^*,\xi^*,\kappa^*$ are material constants due to presence of voids, ∇^2 represents Laplacian operator.

3. Solution procedure

We consider a homogeneous, isotropic micropolar elastic half-space with the void at a non-free surface. The rectangular cartesian coordinate system (x_1, x_2, x_3) having an origin at interface $x_3 = 0$ is considered along with x_3-axis pointing normally into the medium as shown in Fig. 1. Plane waves in x_1-x_3 plane are considered such that the wave-front is parallel to x_2-axis, therefore all the fields variable depend only on x_1, x_3, and t. Thus, the problem is considered two dimensional, so we take

$$\vec{u} = (u_1, 0, u_3), \vec{\phi} = (0, \phi_2, 0). \tag{6}$$

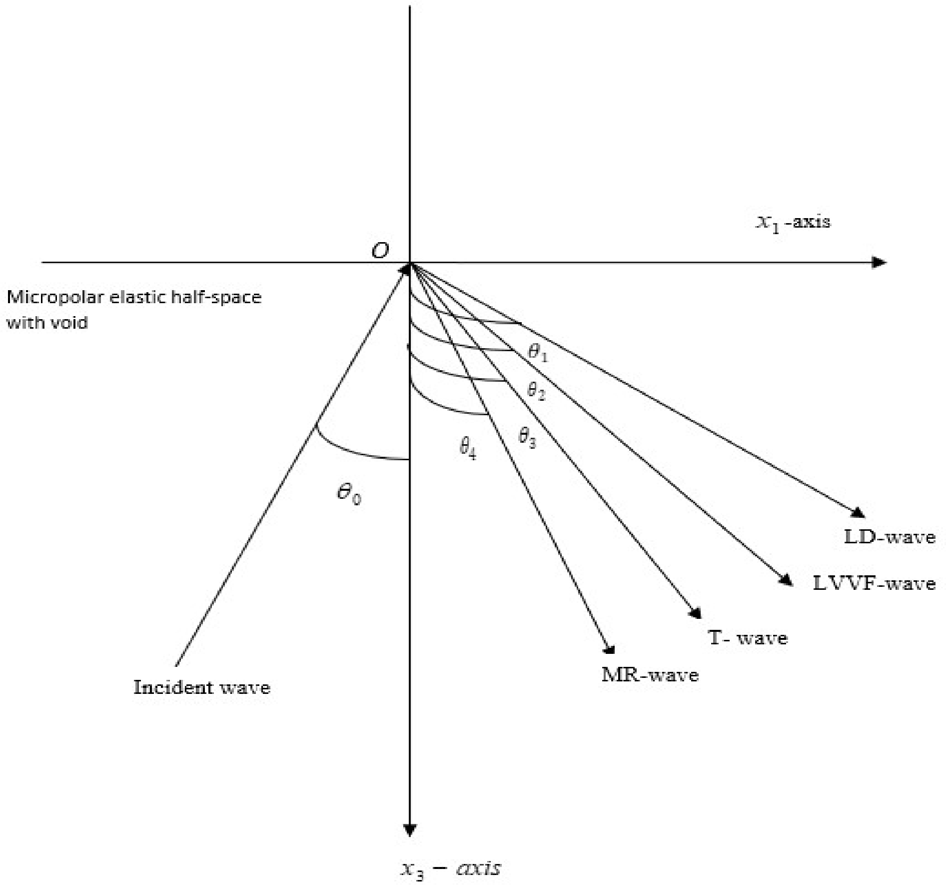

Fig. 1. Geometry of the problem

Dimensionless quantities are taken as

$$(x_i{}', u_i') = \frac{\omega_1}{c_1}(x_i, u_i),\ t'_{3i} = \frac{1}{\mu}t_{3i},\ q' = \frac{K{\omega_1}^2}{c_1^2}q,\ t' = \omega_1 t,\ \phi'_2 = \frac{\hat{j}{\omega_1}^2}{c_1^2}\phi_2,$$

$$m'_{3_2} = \frac{\hat{j}\omega_1}{\gamma c_1}m_{32},\ (i = 1,3) \tag{7}$$

where

$c_1^2 = \frac{\lambda+2\mu+K}{\rho}$ and ${\omega_1}^2 = \frac{K}{\rho\hat{j}}$.

Making use of equations (6)-(7) in equations (1)-(5), we obtain

$$a_1\frac{\partial}{\partial x_1}\left(\frac{\partial u_1}{\partial x_1} + \frac{\partial u_3}{\partial x_3}\right) + a_2\nabla^2 u_1 - a_3\frac{\partial \phi_2}{\partial x_3} + a_4\frac{\partial q}{\partial x_1} = \frac{\partial^2 u_1}{\partial t^2}, \tag{8}$$

$$a_1\frac{\partial}{\partial x_3}\left(\frac{\partial u_1}{\partial x_1} + \frac{\partial u_3}{\partial x_3}\right) + a_2\nabla^2 u_3 + a_3\frac{\partial \phi_2}{\partial x_1} + a_4\frac{\partial q}{\partial x_3} = \frac{\partial^2 u_3}{\partial t^2}, \tag{9}$$

$$a_5\nabla^2\phi_2 + a_6\left(\frac{\partial u_1}{\partial x_3} - \frac{\partial u_3}{\partial x_1}\right) - a_7\phi_2 = \frac{\partial^2\phi_2}{\partial t^2}, \tag{10}$$

$$a_{13}\nabla^2 q - a_{14}q - a_{15}\frac{\partial q}{\partial t} - a_{16}\left(\frac{\partial u_1}{\partial x_1} + \frac{\partial u_3}{\partial x_3}\right) = \frac{\partial^2 q}{\partial t^2}, \tag{11}$$

$$t_{33} = a_8\frac{\partial u_1}{\partial x_1} + a_9\frac{\partial u_3}{\partial x_3} + a_{10}q, \tag{12}$$

$$t_{31} = a_{11}\frac{\partial u_1}{\partial x_3} + \frac{\partial u_3}{\partial x_1} - a_{12}\phi_2, \tag{13}$$

$$m_{32} = \frac{\partial \phi_2}{\partial x_3}, \tag{14}$$

where

$a_1 = \frac{\lambda+\mu}{\rho c_1^2}$, $a_2 = \frac{\mu+K}{\rho c_1^2}$, $a_3 = \frac{K}{\hat{j}\rho\omega_1^2}$, $a_4 = \frac{\beta^*}{\omega_1\hat{j}\rho}$, $a_5 = \frac{\gamma}{\rho c_1^2\hat{j}}$, $a_6 = \frac{K}{\rho c_1^2}$, $a_7 = \frac{2K}{\hat{j}\rho\omega_1^2}$, $a_8 = \frac{\lambda}{\mu}$, $a_9 = \frac{\lambda+2\mu+K}{\mu}$,

$a_{10} = \frac{\beta^* c_1^2}{\mu\hat{j}\omega_1^2}$, $a_{11} = \frac{\mu+K}{\mu}$, $a_{12} = \frac{Kc_1^2}{\mu\hat{j}\omega_1^2}$, $a_{13} = \frac{\alpha^*}{\kappa^*\rho c_1^2}$, $a_{14} = \frac{\xi^*}{\kappa^*\rho\omega_1^2}$, $a_{15} = \frac{\omega^*}{\kappa^*\rho\omega_1^2}$, $a_{16} = \frac{\beta^*\hat{j}}{\kappa^*\rho c_1^2}$.

With the help of the expression given by Helmholtz decomposition, u_1 and u_3 can be expressed as

$$u_1 = \frac{\partial \varphi}{\partial x_1} - \frac{\partial \psi}{\partial x_3},\ u_3 = \frac{\partial \varphi}{\partial x_3} + \frac{\partial \psi}{\partial x_1}. \tag{15}$$

By applying equation (15) in equations (8)-(11), we get

$$\left(\nabla^2 - \frac{\partial^2}{\partial t^2}\right)\varphi + a_4 q = 0, \tag{16}$$

$$\left(a_2\nabla^2 - \frac{\partial^2}{\partial t^2}\right)\psi + a_3\phi_2 = 0, \tag{17}$$

$$\left(a_5\nabla^2 - \frac{\partial^2}{\partial t^2} - a_7\right)\phi_2 - a_6\nabla^2\psi = 0, \tag{18}$$

$$\left(a_{13}\nabla^2 - \frac{\partial^2}{\partial t^2} - a_{14} - a_{15}\frac{\partial}{\partial t}\right)q - a_{16}\nabla^2\varphi = 0. \tag{19}$$

Assuming the motion to be harmonic and for solving the equations (16)-(19), we assume the solutions as

$$(\varphi, q, \psi, \phi_2) = (\varphi^o, q^o, \psi^o, {\phi_2}^o)e^{\iota\kappa(x_1\sin\theta_0 - x_3\cos\theta_0 + \nu t)}, \tag{20}$$

where κ denotes as a wave number, ι is known as iota, θ_0 is the angle of inclination, and quantities such as φ^o, q^o, ψ^o and ${\phi_2}^o$ are arbitrary constants. Using the values of φ, q, ψ, and ϕ_2, we obtained the following equations

$$(\nu^4 + A_{01}\nu^2 + A_{02})(\varphi, q) = 0, \tag{21}$$

$$(\nu^4 + A_{03}\nu^2 + A_{04})(\psi, \phi_2) = 0, \tag{22}$$

where $\nu = \left(\frac{\omega}{\kappa}\right)$ denotes the velocity of waves, ν_i $(i = 1-4)$ are velocities of the LD-wave, LVVF-wave, T-wave, and MR-wave respectively and

$A_{01} = \frac{-(a_4a_{16} - a_{14} + (a_{13}+1)\omega^2 + \iota\omega a_{15})}{\omega^2 - a_{14} + \iota\omega a_{15}}$, $A_{02} = \frac{a_{13}\omega^2}{\omega^2 - a_{14} + \iota\omega a_{15}}$, $A_{03} = \frac{a_2a_7 - a_3a_6 - (a_5+a_2)\omega^2}{\omega^2 - a_7}$,

$A_{04} = \frac{a_2a_5\omega^2}{\omega^2 - a_7}$.

4. Boundary conditions

For the free surface, the component of stresses is zero but for the non-free surface, some finite values may exist and they are proportionate to the components of displacement as well as rotational components, and appropriate conditions at $x_3 = 0$ are

$$\text{(i) } t_{33} = -\iota S_1 u_3,\ \text{(ii) } t_{31} = -\iota S_2 u_1,\ \text{(iii) } m_{32} = -\iota S_3\phi_2,\ \text{(iv) } \frac{\partial q}{\partial x_3} = 0. \tag{23}$$

In equation (23) S_1, S_2, and S_3 represent the stiffness along the normal component, tangential component, and rotational component. The stress field and displacement field are expressed in terms of complex quantities as it is observed that there is a phase shift between the stress field and displacement field due to the mathematical relation $u_{ij} = \iota\kappa_j u_i$ but actually, extra phase shift does not exist so to overcome this extra phase shift effect, we introduced a negative unit, $-\iota$ into the right side of equation (23).

5. Reflection at the non-free surface

To obtain amplitude ratio at non-free surface we consider φ, q, ψ, and ϕ_2 as follows:

$$\varphi = \sum A_{0i}\, e^{\iota\kappa_0(x_1\sin\theta_0 - x_3\cos\theta_0) + \iota\omega t} + A_i e^{\iota\kappa_i(x_1\sin\theta_i + x_3\cos\theta_i) + \iota\omega t}, \tag{24}$$

$$q = \sum d_i\left(A_{0i}e^{\iota\kappa_0(x_1\sin\theta_0 - x_3\cos\theta_0)+\iota\omega t} + A_i e^{\iota\kappa_i(x_1\sin\theta_i + x_3\cos\theta_i)+\iota\omega t}\right), \tag{25}$$

$$\psi = \sum B_{0i}\, e^{\iota\kappa_0(x_1\sin\theta_0 - x_3\cos\theta_0)+\iota\omega t} + B_i e^{\iota\kappa_j(x_1\sin\theta_j + x_3\cos\theta_j)+\iota\omega t}, \tag{26}$$

$$\phi_2 = \sum f_i\left(B_{0i}e^{\iota\kappa_0(x_1\sin\theta_0 - x_3\cos\theta_0)+\iota\omega t} + B_i e^{\iota\kappa_j(x_1\sin\theta_j + x_3\cos\theta_j)+\iota\omega t}\right), \tag{27}$$

where

$$d_i = \frac{\omega^2 - \kappa_i{}^2}{a_4},\ f_i = \frac{a_5\kappa_j^2 + a_7 - \omega^2}{a_6\kappa_j^2}, (i = 1,2), (j = 3,4),$$

where $A_{0i}\,(i = 1,2)$ are the amplitude of incident LD-wave, LVVF-wave, and $B_{0i}(i = 1,2)$ are the amplitude of incident T-wave and MR-wave. A_i are the amplitude of the reflected LD-wave and LVVF-wave. B_i are the amplitude of the reflected T-wave and reflected MR-wave.

Snell's Law is given by

$$\frac{\sin\theta_0}{\upsilon_0} = \frac{\sin\theta_i}{\upsilon_i}, \tag{28}$$

where

$$\kappa_i\upsilon_i = \omega, \text{ at } x_3 = 0\ (i = 1-4), \tag{29}$$

$$\upsilon_0 = \begin{cases} \upsilon_1, & \text{incident LD} - \text{wave} \\ \upsilon_2, & \text{incident LVVF} - \text{wave} \\ \upsilon_3, & \text{incident T} - \text{wave} \\ \upsilon_4, & \text{incident MR} - \text{wave} \end{cases}$$

Considering the phase of the reflected waves and using the equations (28)-(29), we can write,

$$\frac{\cos\theta_j}{\upsilon_j} = \left[\left(\frac{\upsilon_0}{\upsilon_j}\right)^2 - \sin^2\theta_0\right]^{\frac{1}{2}}. \tag{30}$$

As given by Schoenberg [26], we can write,

$$\frac{\cos\theta_j}{\upsilon_j} = \frac{\cos\overline{\theta_j}}{\overline{\upsilon_j}} + \iota\frac{c_j}{2\pi\upsilon_0}, \qquad (j = 1-4),$$

$$\frac{\cos\overline{\theta_j}}{\overline{\upsilon_j}} = \frac{1}{\upsilon_0}R_e\left\{\left[\left(\frac{\upsilon_0}{\upsilon_j}\right)^2 - \sin^2\theta_0\right]^{\frac{1}{2}}\right\},\quad c_j = 2\pi I_m\left[\left(\frac{\upsilon_0}{\upsilon_j}\right)^2 - \sin^2\theta_0\right]^{\frac{1}{2}},$$

where $\overline{\upsilon_j}$ and $\overline{\theta_j}$ denote the real phase speed and the angle of reflection respectively. c_j represent the attenuation in a depth and it is assumed to be equal to the wavelength of the incident wave i.e. $(2\pi\upsilon_0)/\omega$,

$$\frac{\overline{\upsilon_j}}{\upsilon_0} = \frac{\sin\overline{\theta_j}}{\sin\theta_0}\left[\sin^2\theta_0 + \left[R_e\left(\left[(\upsilon_0\upsilon_4)^2 - \sin^2\theta_0\right]^{\frac{1}{2}}\right)\right]^2\right]^{\frac{-1}{2}}.$$

Invoking the boundary conditions (23) along the equations (12)-(14), (15) and using the values of $\varphi, q, \psi,$ and ϕ_2 from equations (24)-(27) along with equation (30), we obtained following system of equations as

$$\sum b_{ij}\,R_j = Y_{j,} \qquad (i,j = 1-4), \tag{31}$$

$$b_{1p} = -d_p\left[\left[a_8\left(\frac{\upsilon_p}{\upsilon_0}\right)^2\sin^2\theta_0 + a_9\left(\frac{\upsilon_p}{\upsilon_0}\right)^2\left[\left(\frac{\upsilon_0}{\upsilon_p}\right)^2 - \sin^2\theta_0\right]\right]\kappa_p^2 + a_{10} - \kappa_p d_p S_1\left[\left(\frac{\upsilon_0}{\upsilon_p}\right)^2 - \sin^2\theta_0\right]^{\frac{1}{2}}\right],$$

$$b_{1q} = f_p \sin\theta_0 \left[\kappa_q^2(a_8 - a_9)\left(\frac{\upsilon_q}{\upsilon_0}\right)^2\left[\left(\frac{\upsilon_0}{\upsilon_q}\right)^2 - \sin^2\theta_0\right]^{\frac{1}{2}} - \kappa_q S_1 \frac{\upsilon_q}{\upsilon_0}\right],$$

$$b_{2p} = -d_p\kappa_p^2 \sin\theta_0 (a_{11}+1)\left(\frac{\upsilon_p}{\upsilon_0}\right)^2\left[\left(\frac{\upsilon_0}{\upsilon_p}\right)^2 - \sin^2\theta_0\right]^{\frac{1}{2}} - d_p\kappa_p S_2 \frac{\upsilon_p}{\upsilon_0}\sin\theta_0,$$

$$b_{2q} = f_p\kappa_q^2\left[a_{11}\left(\frac{\upsilon_q}{\upsilon_0}\right)^2\left[\left(\frac{\upsilon_0}{\upsilon_q}\right)^2 - \sin^2\theta_0\right] - \left(\frac{\upsilon_q}{\upsilon_0}\right)^2 \sin^2\theta_0\right] - a_{12} + f_p\kappa_q S_2 \frac{\upsilon_q}{\upsilon_0}\left[\left(\frac{\upsilon_0}{\upsilon_q}\right)^2 - \sin^2\theta_0\right]^{\frac{1}{2}},$$

$$b_{3p} = \iota\kappa_q \frac{\upsilon_q}{\upsilon_0}\left[\left(\frac{\upsilon_0}{\upsilon_q}\right)^2 - \sin^2\theta_0\right]^{\frac{1}{2}} + \iota S_3,\ b_{3q} = 0,$$

$$b_{4p} = \iota\kappa_p \frac{\upsilon_p}{\upsilon_0}\left[\left(\frac{\upsilon_0}{\upsilon_p}\right)^2 - \sin^2\theta_0\right]^{\frac{1}{2}},\ b_{4q} = 0, \qquad (p = 1,2), (q = 3,4),$$

where R_1, R_2, R_3, and R_4 are the amplitude ratios of reflected LD-wave, LVVF-wave, T-wave, and MR-wave making an angle $\theta_1, \theta_2, \theta_3$, and θ_4 respectively as shown in Fig. 1 and are given by

$$R_1 = \frac{A_1}{A^*}, \quad R_2 = \frac{A_2}{A^*}, \quad R_3 = \frac{B_1}{A^*}, \quad R_1 = \frac{B_2}{A^*}.$$

For incident LD-wave, $A^* = A_{01}$,

$Y_1 = -b_{11}, \quad Y_2 = b_{21}, \quad Y_3 = b_{31}, \quad Y_4 = b_{41}.$

For incident LVVF-wave, $A^* = A_{02}$,

$Y_1 = -b_{12}, \quad Y_2 = b_{22}, \quad Y_3 = b_{32}, \quad Y_4 = b_{42}.$

For incident T-wave, $A^* = B_{01}$,

$Y_1 = b_{13}, \quad Y_2 = -b_{23}, \quad Y_3 = b_{33}, \quad Y_4 = b_{43}.$

For incident MR-wave, $A^* = B_{02}$,

$Y_1 = b_{14}, \quad Y_2 = -b_{24}, \quad Y_3 = b_{34}, \quad Y_4 = b_{44}.$

6. Particular cases

Elastic medium with the void. If $\boldsymbol{\alpha} = \boldsymbol{\beta} = \boldsymbol{\gamma} = \mathbf{K} = \mathbf{0}$, then the above results reduce to elastic media with void having the following changes:

$(\nu^4 + A_{01}\nu^2 + A_{02})(\varphi, q) = 0,$

$(\nu^2 - a_2)\psi = 0,$

where

$$A_{01} = \frac{-(a_4a_{16} - a_{14} + (a_{13}+1)\omega^2 + \iota\omega a_{15})}{\omega^2 - a_{14} + \iota\omega a_{15}}, \qquad A_{02} = \frac{a_{13}\omega^2}{\omega^2 - a_{14} + \iota\omega a_{15}}, \quad a_2 = \frac{\mu}{\rho c_1^2}, \qquad a_9 = \frac{\lambda + 2\mu}{\mu}.$$

Micropolar elastic media. If $\boldsymbol{\alpha}^* = \boldsymbol{\beta}^* = \boldsymbol{\xi}^* = \boldsymbol{\omega}^* = \boldsymbol{\kappa}^* = \mathbf{0}$, then results for reflected waves deduce for micropolar elastic media and following changes are observed,

$(\nu^2 - 1)\varphi = 0,$

$(\nu^4 + A_{03}\nu^2 + A_{04})(\psi, \phi_2) = 0,$

where

$$A_{03} = \frac{a_2a_7 - a_3a_6 - (a_5 + a_2)\omega^2}{\omega^2 - a_7}, \quad A_{04} = \frac{a_2a_5\omega^2}{\omega^2 - a_7}.$$

The above results tally with those obtained by Zhang et al. [22] after substituting appropriate values of the parameters.

7. **Numerical result and discussion**

Following are values of micropolar parameters for numerical computation given by Eringen [27], physical constants are given by [16],

$\lambda = 9.4 \times 10^{10}\mathrm{Nm}^{-2}, \mu = 4 \times 10^{10}\mathrm{Nm}^{-2}, \quad \mathrm{K} = 1.0 \times 10^{10}\mathrm{Nm}^{-2}$,
$\gamma = 0.779 \times 10^{-9}\mathrm{N}, \ \hat{\jmath} = 0.2 \times 10^{-19}\mathrm{m}^2, \rho = 1.74 \times 10^3 \ \mathrm{Kgm}^{-3}$.

The values of the void parameters are taken as

$\alpha^* = 3.688 \times 10^{-9}\ \mathrm{N}, \beta^* = 1.1384 \times 10^{10}\ \mathrm{Nm}^{-2}, \quad \xi^* = 1.147 \times 10^{10}\ \mathrm{Nm}^{-2}$,
$\kappa^* = 1.175 \times 10^{-19}\mathrm{m}^2, \omega^* = 0.0787 \times 10^{-1}\ \mathrm{Nsm}^{-2}$.

A comparison of values of the amplitude ratios of different reflected waves against the angle of incidence θ_0 is represented graphically for micropolar non-free surface i.e. $S_1 = S_2 = S_3 = 0.5$ (with the void and without void) and for free surface i.e. $S_1 = S_2 = S_3 = 0$ (with the void and without void). The computation for micropolar non-free surface (MNFS) without void is represented by a small dashed line and for micropolar non-free surface (MVNFS) with the void is represented by a small dashed line with center symbols triangle (Δ) respectively. The computation for micropolar free surface (MFS) without void is represented by a solid line and for micropolar free surface (MVFS) with the void is represented by solid with center symbols diamond (⍰) respectively.

Longitudinal displacement (LD)-Wave. Figure 2 demonstrates the trend of $|\mathbf{R_1}|$ vs. $\boldsymbol{\theta_0}$. It is noticed that the magnitude of $|\mathbf{R_1}|$ shows steady state behavior for all the considered cases. It is also observed that in most of the intervals, the magnitude of the values of $|\mathbf{R_1}|$ is slightly greater for MVFS & MVNFS in comparison to MFS & MVFS which depicts the impact of void parameters on amplitude ratios.

Figure 3 depicts the variation of $|R_2|$ vs. θ_0. It is observed that at the beginning, the value of $|R_2|$ for MVFS & MVNFS have greater magnitude as compared with MFS & MNFS respectively but with an increase in θ_0, the trend reversed.

Figure 4 exhibits the plot of $|R_3|$ vs. θ_0. It is noticed that the behavior of $|R_3|$ for all the considered cases follows a similar trend with a significant difference in their magnitude but the magnitude of $|R_3|$ for MFS is higher as compared to other considered cases.

From Figure 5, it is noticed that the value of $|R_4|$ for MVFS and MVNFS increases in the first half of the interval, and later on, the value decreases, and the magnitude of $|R_4|$ is more for MVFS as compared to MVNFS and this difference in magnitude shows the impact of stiffnesses on amplitude ratios.

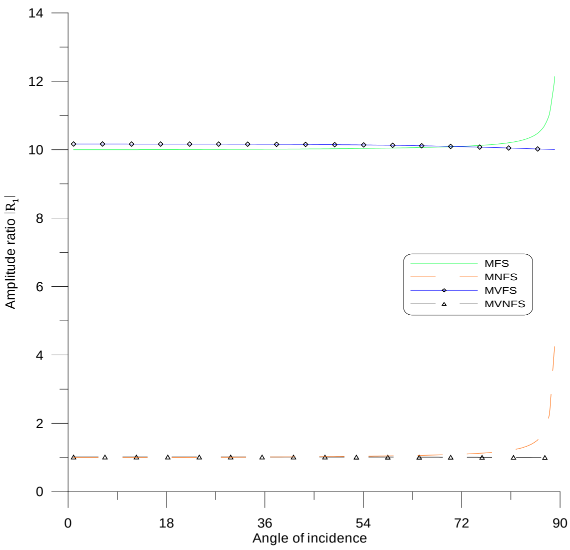

Fig. 2. Variation of Amplitude ratio $|R_1|$ for LD wave

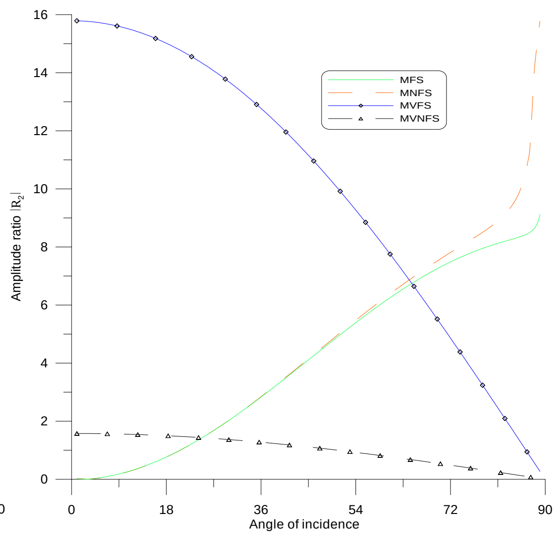

Fig. 3. Variation of Amplitude ratio $|R_2|$ for LD wave

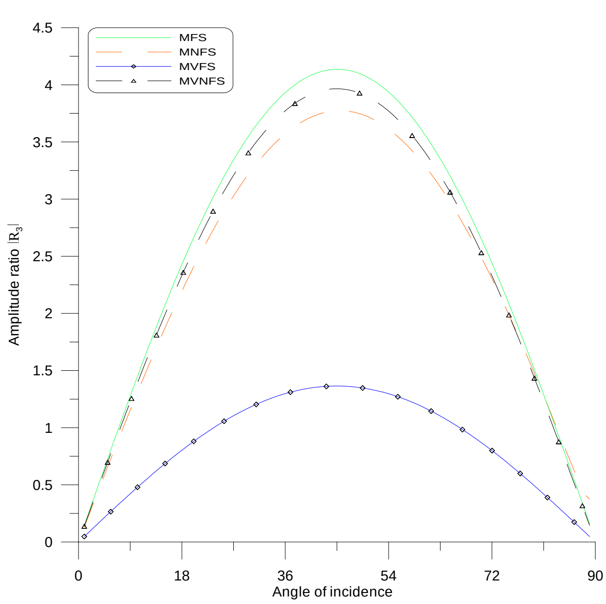

Fig. 4. Variation of Amplitude ratio $|R_3|$ for LD wave

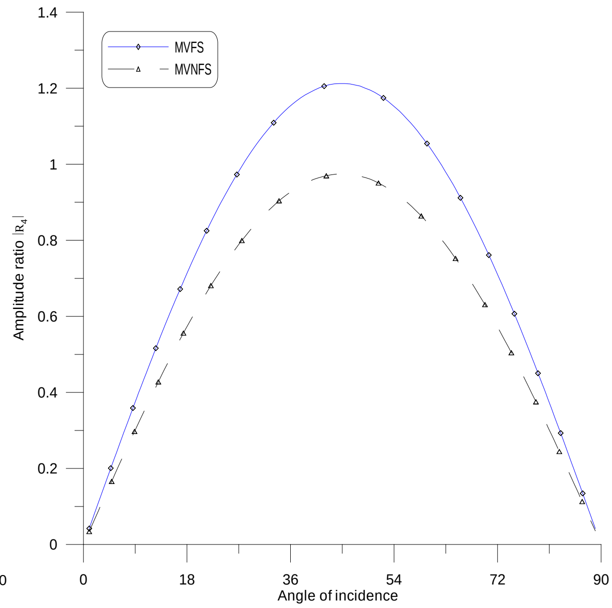

Fig. 5. Variation of Amplitude ratio $|R_4|$ for LD wave

Longitudinal void volume fraction (LVVF)-Wave. The effect of the stiffnesses is notable on amplitude ratios from Fig. 6 in which the value of $|R_1|$ decreases for MVNFS and MVFS as θ_0 increases. It is also noticed that magnitude of $|R_1|$ is greater for MVNFS in comparison to those observed for MVFS.

Figure 7 depicts the variation of $|R_2|$ vs. θ_0. It is noticed that $|R_2|$ follows a similar trend for MVFS and MVNFS i.e. first increases and attains its maximum value at $\theta_0 = 24^o$, then starts decreasing as θ_0 increases. The magnitude of $|R_2|$ is more for MVNFS when compared with MVFS which depicts that stiffnesses play a vital role in amplitude ratios.

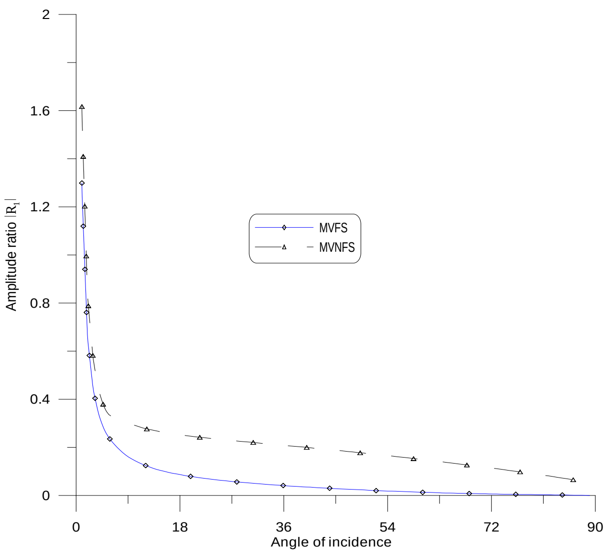

Fig. 6. Variation of Amplitude ratio $|R_1|$ for LVVF wave

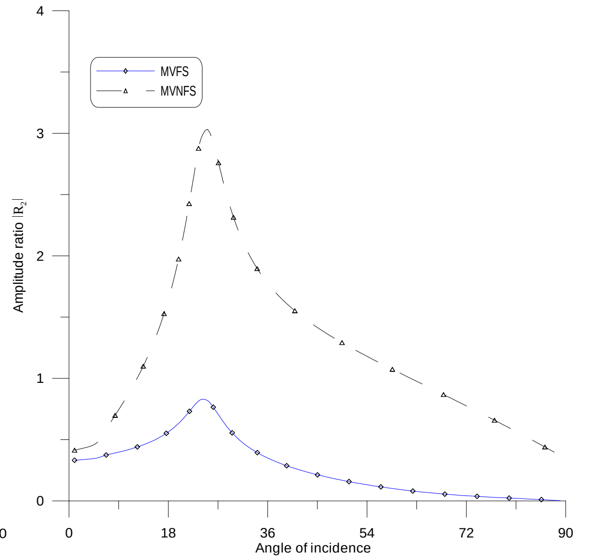

Fig. 7. Variation of Amplitude ratio $|R_2|$ for LVVF wave

Figure 8 shows the variation of amplitude ratio $|R_3|$ vs. θ_0. It is seen that the value of $|R_3|$ for MVNFS & MVFS decreases in the entire range except when $0^o \leq \theta_0 \leq 9^o$, the magnitude of the values of $|R_3|$ are greater for MVNFS in comparison to those obtained for MVFS.

From Figure 9 it is observed that the value of $|R_4|$ for MVNFS decreases for small values of θ_0 and as θ_0 increases, $|R_4|$ shows steady behavior for both MVFS & MVNFS. Due to the presence of stiffness the magnitude of the values of $|R_4|$ for MVNFS is smaller as compared to MVFS.

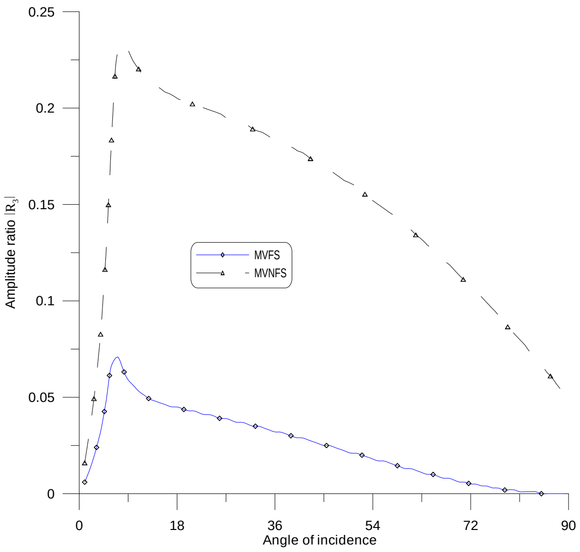

Fig. 8. Variation of Amplitude ratio $|R_3|$ for LVVF wave

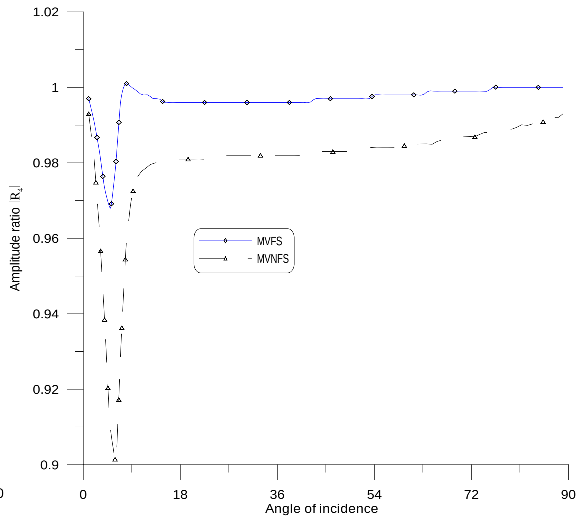

Fig. 9. Variation of Amplitude ratio $|R_4|$ for LVVF wave

Transverse (T)-Wave. Figure 10 depicts the variation of $|R_1|$ vs. θ_0. It is noticed that in absence of void effect i.e. for MFS & MNFS the value of $|R_1|$ shows a decreasing trend in the entire range whereas for MVFS and MVNFS, it shows a vice-versa trend in the entire interval except when $0^o \leq \theta_0 \leq 10^o$.

Figure 11 shows the variation of $|R_2|$ vs. θ_0. It is seen that $|R_2|$ shows ascending trend for MFS in the first half of the interval and vice-versa trends are noticed in the left over the interval whereas due to the presence of stiffnesses, $|R_2|$ for MNFS shows an increasing trend in $0^o \leq \theta_0 \leq 18^o$ and descending behavior in the rest of the interval. It is also observed that $|R_2|$ shows steady state behaviour for MVFS & MVNFS and increases sharply as $\theta_0 \geq 80^o$.

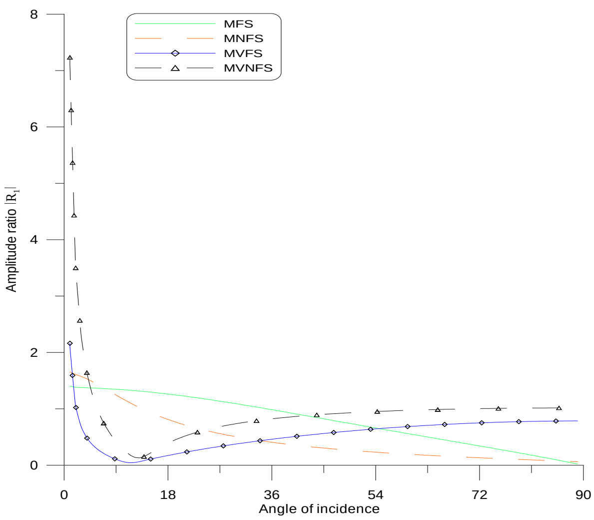

Fig. 10. Variation of Amplitude ratio $|R_1|$ for T wave

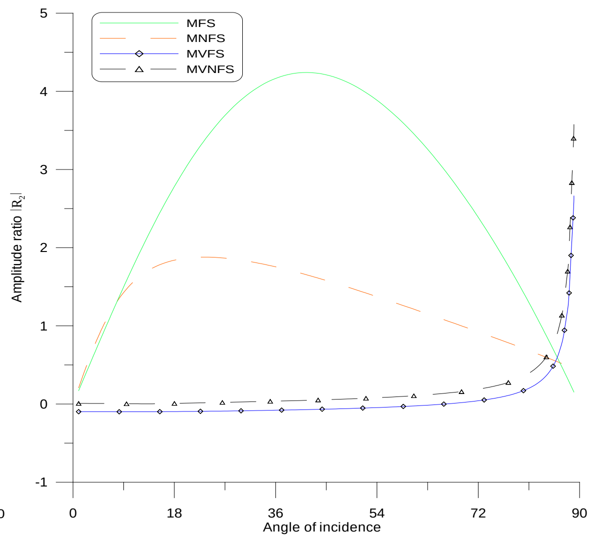

Fig. 11. Variation of Amplitude ratio $|R_2|$ for T wave

Figure 12 depicts the variation of $|R_3|$ vs. θ_0. The value of $|R_3|$ for MFS and MNFS shows descending behavior in the first half of the interval and then increases in the rest half of the interval, whereas $|R_3|$ follows a similar trend for MVFS and MVNFS i.e. increases near the boundary and decreases afterward, magnitude of $|R_3|$ is greater for MVFS.

From Figure 13, it is noticed that the value of $|R_4|$ for MVNFS and MVFS decreases for $0^o \leq \theta_0 \leq 10^o$, and the magnitude of $|R_4|$ for both the cases shows ascending trend for the rest of the interval. It is also noticed that the magnitude of $|R_4|$ for MVFS is more than that of MVNFS.

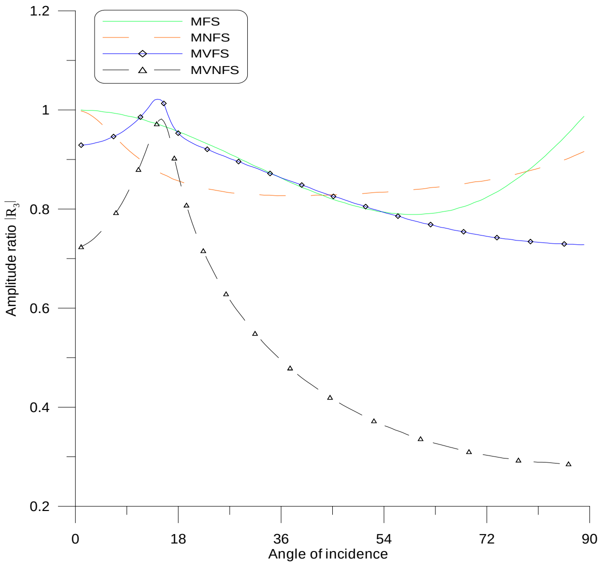

Fig. 12. Variation of Amplitude ratio $|R_3|$ for T wave

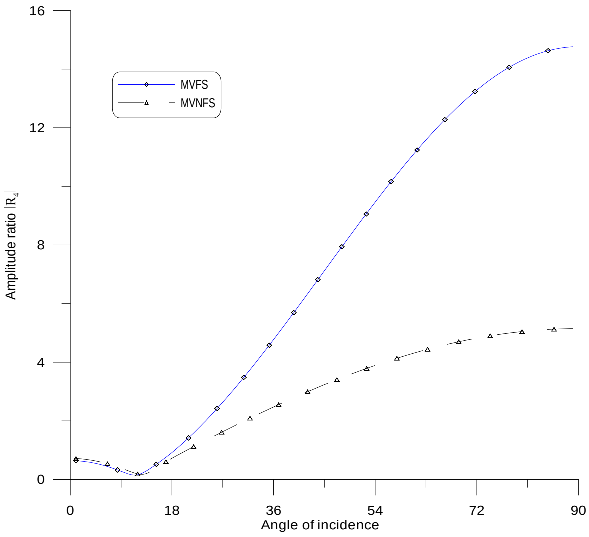

Fig. 13. Variation of Amplitude ratio $|R_4|$ for T wave

Micro-rotational (MR)-Wave. Figure 14 depicts the variation of $|R_1|$ vs. θ_0. It is observed that the value of $|R_1|$ for MFS and MNFS shows small variations about the origin in the interval $0^o \leq \theta_0 \leq 80^o$ and then increases left over the interval whereas the trend of $|R_1|$ for MVFS and MVNFS is increasing in nature due to the presence of stiffness parameters.

In Figure 15, it is noticed that the value of $|R_2|$ shows a steady state for all the considered cases in $0^o \leq \theta_0 \leq 50^o$ and as θ_0 increases, $|R_2|$ for MVFS & MVNFS shows decreasing behavior while $|R_2|$ for MFS & MNFS shows the opposite trend as observed for MVFS & MVNFS.

Figure 16 depicts the value of $|R_3|$ for MVNFS and MVFS increases in the $0^o \leq \theta_0 \leq 54^o$ and decreases in the remaining range, the magnitude of MVNFS is more than MVFS which reveals the impact of the non-free surface on amplitude ratios. A similar impact of stiffnesses can be observed for the values of MNFS and MFS as the magnitude of $|R_3|$ for MNFS is more than MFS with ascending behavior.

From Figure 17, it is noticed that initially the value of $|R_4|$ for MVFS and MVNFS increases and it reaches the maximum at $\theta_0 = 54^o$ and then decreases with an increase in θ_0, the magnitude of amplitude ratio $|R_4|$ for MVFS is more than that of MVNFS.

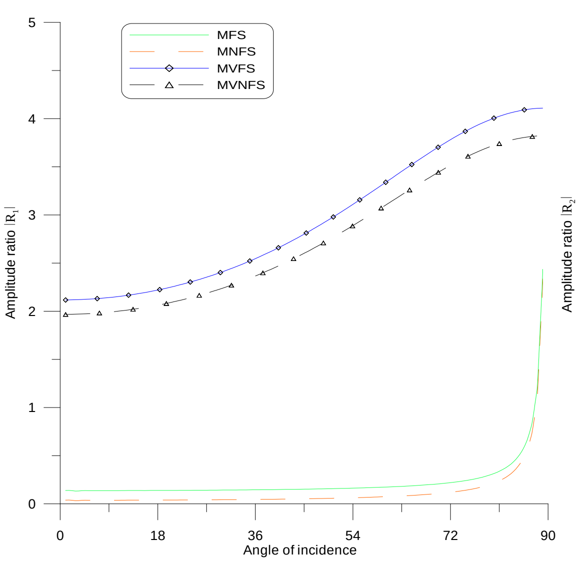

Fig. 14. Variation of Amplitude ratio $|R_1|$ for MR wave

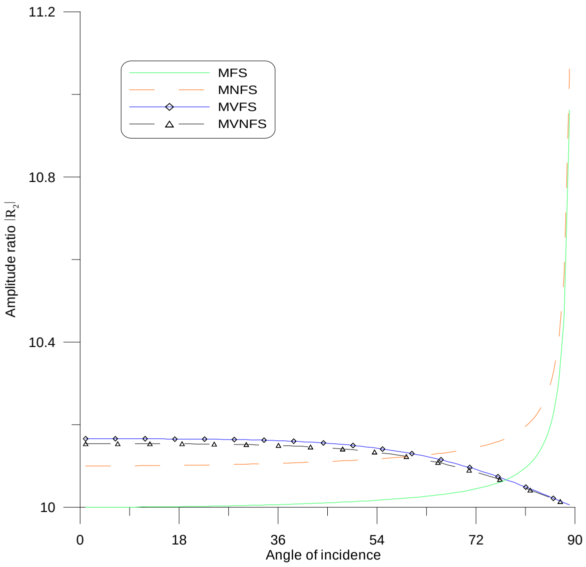

Fig. 15. Variation of Amplitude ratio $|R_2|$ for MR wave

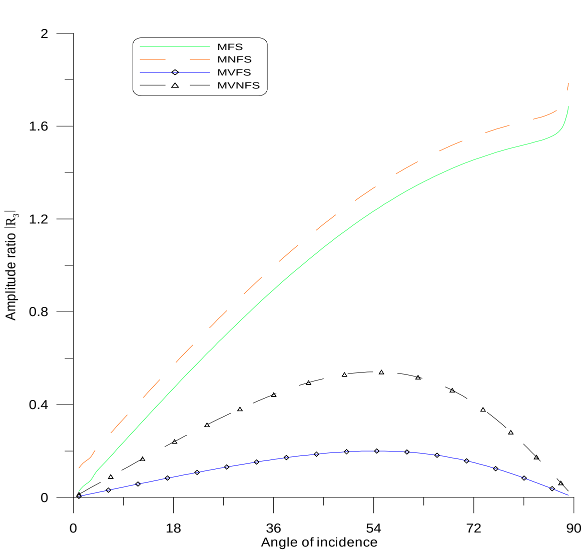

Fig. 16. Variation of Amplitude ratio $|R_3|$ for MR wave

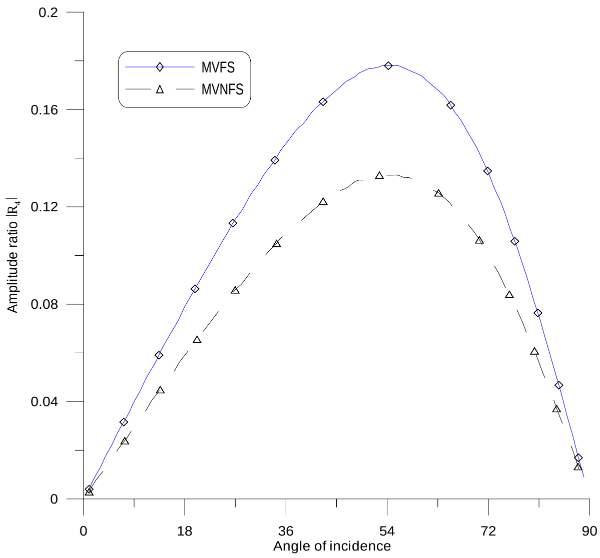

Fig. 17. Variation of Amplitude ratio $|R_4|$ for MR wave

8. Conclusion

In the present article, the phenomenon of reflection of the elastic wave at a non-free surface with a micropolar elastic constraint with void has been studied. The amplitude ratios of four reflected waves namely LD-wave, LVVF-wave, T-wave, and MR-wave are calculated numerically. The impact of stiffnesses and void parameters on these amplitude ratios are demonstrated graphically. From the numerically computed results following observations are made:

(a) The results indicate that due to the presence of stiffnesses, the magnitude of $|R_1|$ and $|R_2|$ is smaller as compared to those obtained for free surface, whereas in the case of $|R_3|$ and $|R_4|$, it shows similar oscillatory behaviour with a significant difference in their magnitude when LD-wave is incident.

(b) It is observed that when LVVF-wave is incident, the magnitudes of $|R_1|$, $|R_2|$, and $|R_3|$ in the case of free surface are smaller while $|R_4|$ shows a vice-versa trend which depicts the significant impact of stiffnesses on amplitude ratios.

(c) In the case of incident T-wave, it is observed that void parameters play a vital role in amplitude ratios as $|R_1|$ and $|R_2|$ show opposite behaviour for MVFS & MVNFS as compared to MFS & MNFS, while in the case of $|R_3|$ and $|R_4|$ they show similar behavior in the entire range.

(d) It is seen that when MR-wave is an incident, void and stiffness parameters play a major role as the magnitude of $|R_1|$, $|R_2|$, and $|R_4|$ for MVFS are greater as compared to MVNFS. It is also noticed that in absence of a void parameter trends are reversed i.e. values of $|R_2|$ and $|R_3|$ for the non-free surface are greater as compared to the free surface.

The physical application of this model can be found in the area of seismology where the results are helpful for the exploration of valuable materials such as minerals, crystals, and metals. The results are also useful in geophysics and earthquake engineering.

References

[1] Abd-Alla AN, Abbas IA. A problem of generalized Magneto-thermoelasticity for an infinitely long, perfectly conducting cylinder. *Journal of Thermal Stresses.* 2002;25(11): 1009-1025.

[2] Abbas IA, Abd-Alla, AN, Othman MIA. Generalized Magneto-thermoelasticity in a Fiber-Reinforced Anisotropic Half-Space. *International Journal of Thermophysics*. 2011;32: 1071-1085.

[3] Abbas IA, Abo-Dahab SM. On the Numerical Solution of Thermal Shock Problem for Generalized Magneto-Thermoelasticity for an Infinitely Long Annular Cylinder with Variable Thermal Conductivity. *Journal of Computational and Theoretical Nanoscience*. 2014;11(3): 607-618.

[4] Hobiny AD, Abbas IA. A study on photothermal waves in an unbounded semiconductor medium with cylindrical cavity. *Mechanics of Time-Dependent Materials*. 2017;21: 61-72.

[5] Hobiny A, Abbas IA. Analytical solutions of photo-thermo-elastic waves in a non-homogenous semiconducting material. *Results in Physics*. 2018;10: 385-390.

[6] Vlase S, Marin M, Ochsner A, Scutaru ML. Motion equation for a flexible one-dimensional element used in the dynamical analysis of a multibody system. *Continuum Mechanics and Thermodynamics*. 2019;31: 715-724.

[7] Omar AA, Shawagfeh N. Application of reproducing kernel algorithm for solving dirichlet time-fractional diffusion-gordon types equations in porous media. *Journal of Porous Media.* 2019;22(4): 411-434.

[8] Saeed T, Abbas IA, Marin M. A GL Model on Thermo-Elastic Interaction in a Poroelastic Material Using Finite Element Method. *Symmetry.* 2020;12(3): 488.

[9] Nunziato JW, Cowin SC. A non-linear theory of elastic material with voids. *Archives of Rational Mechanics and Analysis.* 1979;72: 175-201.

[10] Cowin SC, Nunzaito JW. Linear elastic material with voids. Journal of Elasticity 1984;13: 125-147.

[11] Kumar R, Choudhary S. Interaction due to mechanical sources in micropolar elastic medium with voids. *Journal of Sound and Vibration*. 2003;266: 889-904.

[12] Tomar SK. Wave propagation in a micropolar elastic plate with voids. *Journal of Vibration and Control.* 2005;11: 849-863.

[13] Mondal AK, Acharya DP. Surface waves in a micropolar elastic solid containing voids. *Acta Geophysica*. 2006;54(4): 430-452.

[14] Hsia SY, Cheng JW. Longitudinal plane wave propagation in elastic-micropolar porous media. *Japanese Journal of Applied Physics.* 2006;45(3A): 1743-1748.

[15] Mahmoud SR, Abd-Alla AM, El-Sheikh MA. Effect of the rotation on wave motion through cylindrical bore in a micropolar porous medium. *International Journal of Modern Physics B.* 2011;25(20): 2713-2728.

[16] Singh R, Singh K. Eigen value approach in micropolar elastic medium with voids. International. *Journal of Applied Mechanics and Engineering*. 2013;18(2): 521-536.
[17] Marin M. An approach of a heat-flux dependent theory for micropolar porous media. *Meccanica*. 2016;51: 1127-1133.
[18] Lianngenga, R.: Effect of inertial coefficients in the propagation of plane waves in micropolar porous materials. *International Journal of Computational Materials*. 2017;6(1): 1750007.
[19] Kumari N, Kaliraman V. Analysis of wave propagation at an imperfect boundary between micropolar elastic solid and micropolar porous elasticsolid. *International Journal of Mathematics Trends and Technology*. 2018;53(1): 22-37.
[20] Marin M, Chirila A, Ochsner A, Vlase S. About finite energy solutions in thermoelasticity of micropolar bodies with voids. *Boundary Value Problems*. 2019;2019: 89.
[21] Alharbi AM, Abd-Elaziz EM, Othman MIA. Effect of temperature-dependent and internal heat source on a micropolar thermoelastic medium with voids under 3PHL model. *ZAMM*. 2021;101(6): e202000185.
[22] Zhang P, Wei P, Tang Q. Reflection of micropolar elastic waves at the non-free surface of a micropolar elastic half-space. *Acta Mechanica*. 2015;226: 2925-2937.
[23] Singh B. Reflection of thermoelastic waves at a non-free thermally insulated surface. *International Journal of Applied Science and Engineering*. 2018;15(3): 149-161.
[24] Eringen AC. Theory of micropolar elasticity in fracture. *Academic Press*. 1968;2: 621-729.
[25] Iesan DA. Shock waves in micropolar elastic materials with voids. *Analele Stiintifice ale Universitatu Al. l. Cuzadin lasi Seria Noua Sectiunea la matematica*. 1985;31: 177-186.
[26] Schoenberg M. Transmission and reflection of plane waves at an elastic viscoelastic interface. *Geophysical Journal International*. 1971;25(1-3): 35-47.
[27] Eringen AC. Plane waves in non-local micropolar elasticity. *International Journal of Engineering Science*. 1984;22: 1113-1121.

THE AUTHORS

Kaushal Sachin
e-mail: sachin_kuk@yahoo.co.in
ORCID: 0000-0002-0873-0046

Kumar Rajneesh
e-mail: rajneesh_kuk@rediffmail.com
ORCID: 0000-0000-0000-0001

Kochar Arun
e-mail: arunkochar8@gmail.com
ORCID: 0000-0002-3527-8497